https://doi.org/10.5194/essd-2025-462
Preprint. Discussion started: 26 August 2025

CONFEX: A Database for CONUS Fire EXtent

Raja Zubair Zahoor Qadiri[1,2], Diego Cerrai[1,2]

[1] School of Civil and Environmental Engineering, University of Connecticut, Storrs, CT, USA

[2] Eversource Energy Center, University of Connecticut, Storrs, CT, USA

Corresponding author: Raja Zubair, raja_zubair_zahoor.qadiri@uconn.edu

Abstract. This article presents the CONUS Fire EXtent (CONFEX) database. This database, based on the VIIRS S-NPP 375m data product, provides wildfire perimeter, centroid, ignition location, start and end date for the period 2012 – 2023, for the CONUS and Alaska regions. The algorithm takes hotspot locations from VIIRS S-NPP, clusters them into actual wildfires based on DBSCAN clustering and calculates the perimeter and centroid of each cluster, attaching a geodata frame to each cluster or fire. When validated for some recent large fires against the CALFIRE database, an F1 score of 85 -96% and a CSI of 74 – 93 % were found, showing the efficiency of the algorithm in aggregating hotspots spatially and temporally accurately. This is the first publicly available high-resolution wildfire extent dataset developed for the CONUS and Alaska regions using VIIRS S-NPP 375m data product. The database provides a valuable resource for researchers to understand the complexities of the fire regimes in the CONUS and Alaska regions.

1. Introduction

Wildfire is nature's self-cleansing ritual and a natural part of the carbon cycle (Santín et al., 2015). Natives living in forested regions understood the importance of wildfires and for centuries implemented cultural burning as a duty towards the land that sustained them (Greenler et al., 2024). Overtaking of the native populations led to the exploitation of the forests (Marks-Block & Tripp, 2021). The implementation of fire suppression policies, curtailment of indigenous fire stewardship, mass deforestation of fire-resistant tall trees for fuel purposes, ever increasing thirst for inhabiting wildlands, and on top of that climate change, has led to the current fire pandemic (Martinez et al., 2023; Copes-Gerbitz et al., 2024). In the last two decades fires have raged wrath in the western fire regime of the Continental United States, and their number and severity are expected to increase (Westerling, 2016; Harvey, 2016; Westerling et al., 2006; Iglesias et al., 2022; Holden et al., 2018; Brown et al., 2004). Wildfires have a massive impact on the biosphere. There is a positive feedback loop between climate change and wildfires, with the latter leading to the release of more greenhouse gases, like CO_2 and NO_x, into the atmosphere from biomass burning further aggravating the already hot planet (Barbero et al., 2014). The permafrost thaw and the wildfire regime in the boreal forests create a positive feedback loop, with the former, caused by a changing climate, leading to drier and warmer near surface conditions, increasing fire propagation capacity, and the latter leading to ground subsidence, thickening of the organic content of surface soil layer, changes in the vegetation from coniferous to broad leafed, all leading to increased permafrost thaw (Kim et al., 2024; Kornei, 2020; Li et al., 2021). Massive fires have also led to the intrusion of aerosol into the stratosphere which is causing a slow but steady ozone depletion (Hirsch & Koren, 2021; Ma et al., 2024). At the surface, wildfires destroy the top layer of the soil leading to enhanced erosion and runoff, increasing the probability of flooding events (Wieting et al., 2017).

In this dynamic and ever worsening cycle, researchers have been trying to understand this force of nature, with a massive increase in studies related to wildfires in the last decade. Three prominent areas in this research are predicting the regions ripe for wildfires, especially at the urban wildland interface and along utility distribution lines (Taylor et al., 2024; Barzani et al., 2024; Syphard et al., 2024), real-time wildfire monitoring (Tong et al., 2024; Zhao & Ban, 2025; Briley & Afghah, 2024), and modelling the propagation of an already ignited fire, to effectively dispose of suppression resources (Hu et al., 2024; Sadrabadi & Innocente, 2024; Pereira et al., 2024). These fields need accurate, detailed and global datasets which can be used to study not only the spatial distribution of these fires but also the temporal and spatial evolution of these fires, given the topographic expanse.

Wildfire related data can be acquired through manual or remote sensing methods. Manual methods primarily consist of firefighting units monitoring fires, and of forest service departments surveying burnt areas post fire. After monitoring and surveying, wildfire reports are created based on that information and are made available for public knowledge. The information recorded may include characteristics like probable cause of fire, amount of area burnt, and the extent of damage inflicted (Porter et al., 2019; Brown et al., 2002; Short, 2022). Manual data has been the primary mode for centuries, and for most fires around the urban centers can be reliable in terms of its details about the location of ignition, possible reason, initial mode of spread, and the level and type of discomfort and damage. This provides valuable knowledge for preparing for future fires, through development of more resilient urban infrastructure. However, this data is most accurate at urban or urban wildland interfaces, since that has been the priority for centuries and rightly so. One of such databases is Shorts (2022). This database is one of the most comprehensive ground-based datasets for CONUS, spanning across 28 years from 1992 -2020. The fire entries are manually submitted by local, state and federal organizations.

Remote sensing methods include satellite and low elevation airborne instruments. Broadband spectral sensing and hyperspectral sensing are the two competing surveillance techniques in use currently (Barmpoutis et al., 2020; Dennison & Roberts, 2009; Veraverbeke et al., 2018). Hyperspectral sensing employs a large number (~100) of minute spectral bands (< 0.002 µm) which overlap, while broadband spectral sensing employs a smaller number (3 – 15) relatively larger (>0.002 µm) spread out spectral bands (Veraverbeke et al., 2018). For active fire detection both reside in the short-wave near infrared (1.2 – 2.5 µm) to mid infrared range (3 – 5 µm), where we have a noninterference window, while the nearest infrared (0.7 – 1.2 µm) and visible range (0.4 - 0.7 µm) are not useful due to smoke interference (Veraverbeke et al., 2018). Another spectral range utilized for active fire detection is the thermal infrared band (8 – 12 µm), due to significant fire emissions and the presence of a window in the atmospheric absorption spectrum, however it is close to the earth's average temperature emission peak (~ 9.7 µm). Burnt area mapping is usually done by utilizing the differences in the land cover and moisture differences, and for this microwave spectral region can be utilized especially for negating cloud interferences. Infrared and visible regions are widely employed and are very efficient except for cloud interference (Leblon et al., 2016).

Airborne instruments have been employed for wildfire detection and monitoring since the 1960s. The AAS/5 scanner, onboard the Beechcraft AT 11 aircraft provided useful fire surveillance imagery as early as 1962 (Warren & Wilson, 1981). In 1998 Airborne Visible/Infrared Imaging Spectrometer (AVIRIS) was developed by the Jet Propulsion Laboratory, California Institute of Technology, which has been employed for wildfire surveillance through hyperspectral imaging (Green et al. 1998). In 2008, Airborne Prism experiment (APEX) instrument, another hyperspectral marvel, was developed and has also been employed to the same end (Itten et al. 2008). Since then, development in optics and electronics has led to much more sophisticated instrumentation been applied for wildfire surveillance, techniques like 4π-sr Spectroradiometry, MODIS/ASTER Airborne Simulator (MASTER) scanning spectrometer, and Differential Absorption Lidar - High Spectral Resolution Lidar (DIAL-HSRL), used in the FIREX – AQ mission in 2019 (Warneke et al., 2023). The airborne instruments have high spatial resolution but can only be employed for specific missions because of their limited spatial coverage, the need for a carrier and constant maintenance, making them unfeasible for long-term or large area surveillance. Tower mounted cameras at optimized locations based on terrain in forests for early fire detection has also been a very useful tool (Heyns et al., 2019; Bao et al., 2015). Manual, tower mounted camera-based, and airborne instrument-based monitoring of fire for active fire management are critical since the revisit time of spaceborne instruments is still too large for such advisory (Leblon et al., 2016; Allison et al., 2016).

Satellite fire surveillance came into use a decade and a half after the beginning of the era of meteorological satellites. The quality of satellite-based fire data depends on the orbital type, the instrument used, and the accuracy of the algorithm converting the received signal into actual values. Wildfire-related satellite data has evolved through the years concurrently with the development of satellite technology and computing power. Dozier (1981) provided the basis of the earliest method of extracting remote sensing wildfire data from the passive Advanced Very High-Resolution Radiometer (AVHRR) imagery (3.55 – 3.83 µm and 10.5 -11.5 µm channels) onboard the National Oceanic and Atmospheric Administration (NOAA) managed, NOAA-6 satellite of the Television Infrared Observation Satellite-N series (TIROS-N), facilitated by the presence of two channels in the thermal infrared (IR), primarily intended for sea surface temperature measurements (Nordin & Aziz, 2007). Dozier hypothesized based on the Planck's

https://doi.org/10.5194/essd-2025-462
Preprint. Discussion started: 26 August 2025

radiation law that the temperature difference acquired from the radiation sensed at two different channels at subpixel level is because of varying surface temperature within the pixel rather than interference in the atmosphere and thus can be employed to extract the magnitude and the subpixel spatial fractions of the two temperatures. However, he assumed that there were only two sub-pixel temperatures, a known base (acquired from non-fire pixels), and a target, and this method worked well for unsaturated pixels. However, AVHRR's relatively high resolution meant a lower saturation threshold (450 K over 0.02 Km^2 field of view (FOV)), hindering large fire monitoring, and the NOAA-6 had a single pass each day, making it difficult to track fire progress (Prins & Menzel, 1992). The same algorithm was applied to the imagery (3.9 and 11.2 µm channels) from the Visible Infrared Spin Scan Radiometer Atmospheric Sounder (VAS) on board the NOAA's Geostationary operational environmental satellite (GOES). The coarser resolution (13.8 Km for 3.9 µm and 6.9 km for 11.2 µm), meant that even though it missed small burns, it performed better for large fires due to higher saturation limit (450 K over 5 km^2 FOV). Moreover, as early as 1983, it proved to be a useful tool for monitoring the temporal evolution of wildfires thanks to the hourly data availability (Prins & Menzel, 1992; VAS (1980), n.d.). However, the pixels were still manually checked for fire presence. In 1994 the Cooperative Institute for Meteorological Satellite Studies (CIMSS) developed an automated biomass burning algorithm (ABBA) to classify the VAS pixels for fire, essentially for monitoring basin wide biomass burning over South America, while still relying on the Dozier (1981) method (Prins & Menzel, 1994). The temporal resolution was improved to 15 minutes and the IR resolution was improved to 4 km with the 1994 launch of GOES-8 (Kaufman et al., 1998). The Block 5 Defense meteorological Satellite program (DMSP) satellites were used for providing nighttime monitoring of fires at a 2.7 Km resolution in the 0.4 – 1.1 µm range, as early as 1992 to monitor African savanna burns. However, due to lack of data access the quantification of area was not possible (Cahoon et al., 1992). More detailed information on the early evolution of fire detection techniques using AVHRR onboard NOAA 6 – 14 is provided in the article written by Kaufman et al. (1998). Giglio and Kendall (2001) found that the Dozier algorithm led to ± 50% random error in detecting burnt area and ± 100 K random error in detecting temperature, under sensitivity analysis of fires > 0.05% of the pixel size.

The Moderate Resolution Imaging Spectroradiometer (MODIS) instrument was launched onboard the Earth observing mission (EOM) satellites, terra, in 1999, and aqua, in 2002 (Xiong et al., 2015). The MODIS instrument has 4 special fire channels 2 each for 4 µm and 11 µm, with 500 m spatial resolution, and the algorithm used for its data quantification is provided by Giglio et al. (2003, 2016, 2021). The original MODIS fire detection algorithm, the version 3 or Collection 3, was provided by Kaufman et al. (1998) which suffered high false alarm rate in deserts, or regions of sparse vegetation, and omission of smaller fires. In response to which Collection 4 algorithm was developed by Giglio et al. (2003). Collection 5 product was launched in mid-2006, it has been seen that the threshold for fire detection is high when considered over various terrains and regions and omits fires in some regions (Boschetti et al., 2009). The 310 K 4 µm threshold causes most of the omissions. Even the Collection 5 algorithm struggled with omission of large fires due to thick smoke and falsely generated alarms due to clearing of forests. The Collection 6 and 6.1 algorithm addresses those issues. Offshore gas flaring was also incorporated in the Collection 6 algorithm (Giglio et al. 2016; 2021). The Landsat 7 imagery and Advanced Spaceborne Thermal Emission and Reflection Radiometer (ASTER) imagery are used for validation of the MODIS product. The brightness temperatures from 1 km MODIS channels for 12 µm, 11 µm, and 4 µm are used for deriving the fire product. For sunlight hours, aggregation to 1 km of reflectance of 2.1 µm, 0.85 µm and 0.65 µm are employed. The swath imagery is checked for fire pixels by the algorithm and each pixel is defined as unknown, fire, non-fire, cloud or missing data.

The Visible Infrared Imaging Radiometer Suite (VIIRS) instrument was an upgrade to NASA's AVHRR instrument launched on October 2011 onboard the Suomi National Polar-Orbiting Partnership (S-NPP) and then on NOAA-20 in 2017 and NOAA-21 satellites in November 2022, as part of the EOM (Justice et al., 2013; Cao et al., 2018; Xiong & Butler, 2020; Xiong et al., 2023). The VIIRS has 22 moderate 750 m resolution M bands, and 6 high 375 m resolution I bands. The temporal resolution is 12 h or less, and the threshold for fire detection at nighttime is as low as 5 m^2 (Schroeder et al., 2014).

VIIRS 750 m channel active fire application related product (ARP) was built on the MODIS Collection 4 algorithm, applying the same tests to the VIIRS 750 m multi-spectrum (Justice et al. 2013). In the subsequent upgrades, a pixelated parameter for fire characterization and 2D image classifier were added to the VIIRS 750 m product (Schroeder et al. 2014). VIIRS 750 m product is based on the 4 µm and 11 µm channel data. A new nighttime algorithm

https://doi.org/10.5194/essd-2025-462
Preprint. Discussion started: 26 August 2025

uses the Day-Night Band (DNB) and 1.61 µm channel for sub pixel high temperature and gas flare detection at night (Elvidge et al., 2013).

The VIIRS 375m channels are also used for fire -detection. The product algorithm processes five I band, and one M band given in figure 1. The five channels of I band extend from the mid to thermal infrared region and are thus used for fire detection. I4 (3.55 – 3.93 µm) is the main channel for fire detection and is used to distinguish between subpixel fires and non-fires, with a 367 K saturation temperature (Schroeder et al. 2014). This channel is 0.3 µm below the M13 channel (3.973 – 4.128 µm) that corresponds to the VIIRS 750 m ARP. Channel I5 (10.5 – 12.4 µm) is the thermal channel against which the I4 channel checks for non-fires. The rest of the three channels are used in the algorithm for water body discrimination, sun glint and clouds. For validation of VIIRS 375 imagery, Landsat- 8 data is used.

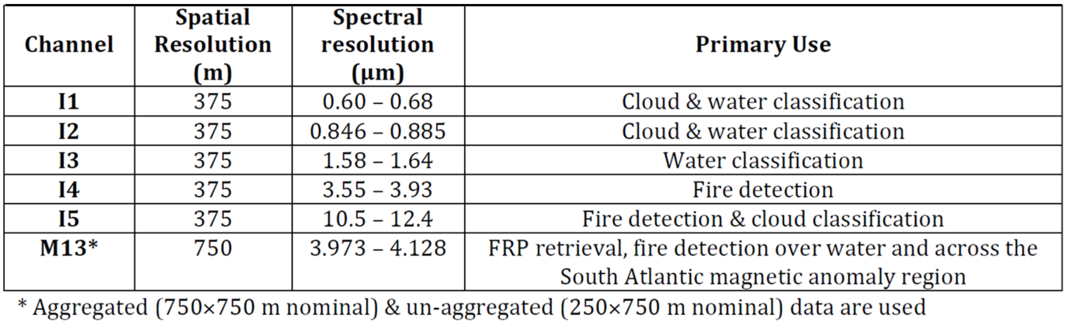

Channel	Spatial Resolution (m)	Spectral resolution (µm)	Primary Use
I1	375	0.60 – 0.68	Cloud & water classification
I2	375	0.846 – 0.885	Cloud & water classification
I3	375	1.58 – 1.64	Water classification
I4	375	3.55 – 3.93	Fire detection
I5	375	10.5 – 12.4	Fire detection & cloud classification
M13*	750	3.973 – 4.128	FRP retrieval, fire detection over water and across the South Atlantic magnetic anomaly region

* Aggregated (750×750 m nominal) & un-aggregated (250×750 m nominal) data are used

Figure 1: Channels used in the 375 m active fire detection algorithm (adapted from Schroeder & Giglio, 2016)

In the current article a wildfire dataset developed based on the VIIRS 375 m active fire product is presented (Qadiri and Cerrai, 2025). The dataset was developed to fill the gaps present in the currently available CONUS datasets. Currently available manual datasets do not provide fire extents over large domains, while the satellite derived datasets either have low spatial resolution due to the raw product used or do not provide fire extent. This product uses a very high resolution VIIRS S-NPP product available on a global scale at high temporal resolution (2 - 4 passes per 12 hours). In this article, section 2 will explain the motivation and methodology behind the evolution of the dataset. Section 3 will explain data characteristics and some case studies to highlight the dataset in detail with examples of some well-known fires.

2. Methodology

2.1 Motivation

The product described in this manuscript was created due to lack of a dependable wildfire dataset product for the Northeast of CONUS. We analyzed the ground-based dataset by Short et al. (2022), and the MODIS and VIIRS satellite pixel products from NASA fire information for resource management system (NASA | LANCE | FIRMS) (Figure 2). The Short database was created to supplement the National fire program analysis (FPA) system. There are some spatial inconsistencies in the Shorts database even though significant improvements have been made to the current version compared to previous versions. It further lacks fire extent or perimeter information. The MODIS and VIIRS S-NPP fire product from NASA FIRMS (NASA | LANCE | FIRMS) were just the fire pixels or hotspots and not actual fires. By comparing the MODIS and the VIIRS products, we found that the number of fire pixels in VIIRS is much higher than the one detected by MODIS due to the higher resolution.

https://doi.org/10.5194/essd-2025-462
Preprint. Discussion started: 26 August 2025

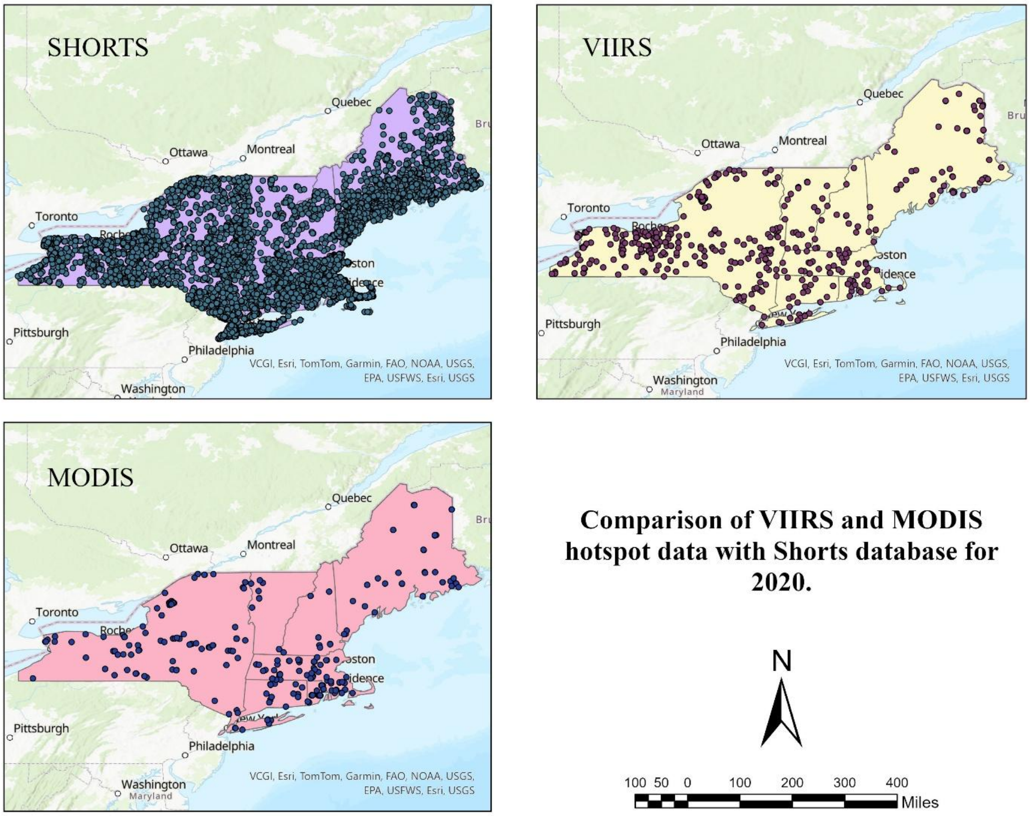

Figure 2 Comparison of short et al (2016) database and MODIS firms hotspot product for the Northeast CONUS for 2001.

To address the shortcomings related to lack of spatial extent, spatial inconsistency, different resolutions and identification of hotspots instead of actual fires, we developed a novel CONUS Fire Extent (CONFEX) product for CONUS and Alaska, based on the VIIRS hotspot or fire pixel data from NASA FIRMS.

The final product was developed for the period 2012- 2023 based on the availability of the NASA FIIRMS data. All the pixels were retained, and the entire CONUS and Alaska were processed. The CONFEX database contains the area, the start date, the end date, the centroid location and perimeter of the fire. The work was aided by some earlier products formed based on MODIS and VIIRS (Artés et al., 2019; Chen et al., 2022) but there is no database of this kind based on VIIRS 375 S-NPP for the CONUS to the authors knowledge.

2.2 Algorithm for the generation of the CONFEX product

The algorithm uses the VIIRS S-NPP 375 m resolution pixel or hotspot data, available from the NASA FIRMS website, as input (Figure 3). The hotspots are first re-projected into a EPSG: 5070 geographic coordinate system, suited for CONUS, to keep as close to the actual distance as possible accommodating the earth's shape at low latitudes. Then, each hotspot is converted into a normalized feature vector. The algorithm then uses DBSCAN to calculate the Euclidean distance and absolute temporal difference in pairs for hotspots and each pair with both values below custom metrics are in the same cluster. The clustering distance threshold for each pair is 750-meter. This comes from the fact that it is twice as much as 375 m, therefore for two tangent circles of radius 375 m, the distance between two points is 750 m. The clustering temporal distance threshold is 120-hour, which is based on the fact that we assumed absence of a fire, if no fire is detected over multiple overpasses in a period of 5 days. Once the clustering is done, if the cluster contains more than 3 hotspots, Delaunay triangulation is performed, keeping the triangles in which the circumradius is not more than 1/∞. Finally, polygonization of the filtered triangles is performed to assign an alpha shape to the cluster (concave hull) which has been previously used by other researchers for assigning shapes to fire clusters (Chen et al., 2022). For clusters containing less than 3 hotspots, convex hull is used to assign shapes. After assigning the shapes, the areas of the resultant concave or convex polygons are calculated. The resultant polygon is saved as a shape file for each fire cluster. The resultant data set is composed of geodata frames assigned to each cluster, with attributes of ignition time and date, end time and date, area, ignition latitude, ignition longitude, centroid latitude, and centroid longitude. Moreover, a csv file in which each row corresponds to the summary of all the important attributes of one cluster's geodata frame is also created. This summary file also contains the cluster ID which can be used to locate the shapefile with the same ID name.

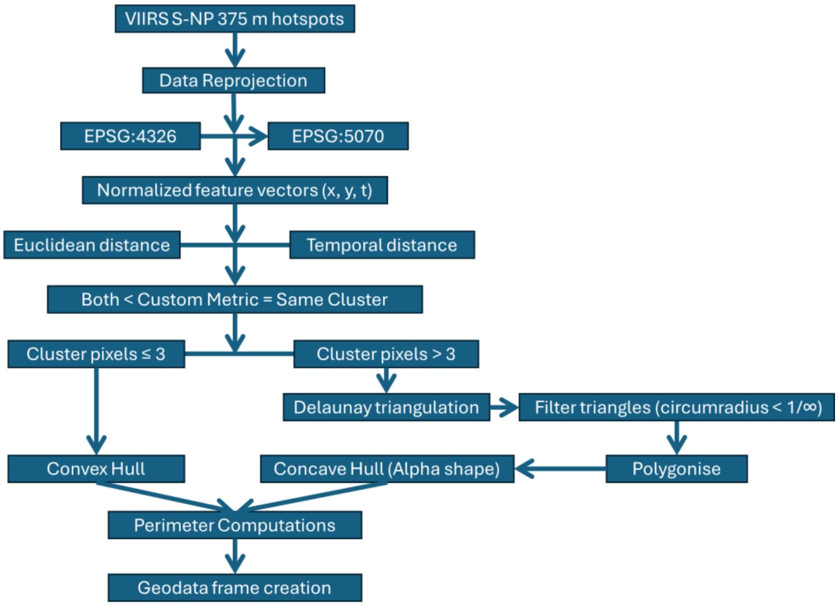

Figure 3 Algorithm for developing CONFEX from VIIRS S-NPP 375 m data.

3. Dataset characteristics

In this section, we analyzed the CONFEX database to provide an overview of its spatial and temporal characteristics and highlight its strengths and limitations. From a time series of the newly developed CONFEX summary database computed over the CONUS area and Alaska, it is possible to find that the year characterized by the largest burnt area was 2020, with 38844.96 Km^2, followed by 2021 (Figure 4 a). The fire season is bimodal with one peak in March and the other in October (Figure 4 b). It is also possible to notice a very high interannual variability. As an example, the burnt area in 2023 has been less than half the activity in 2020.

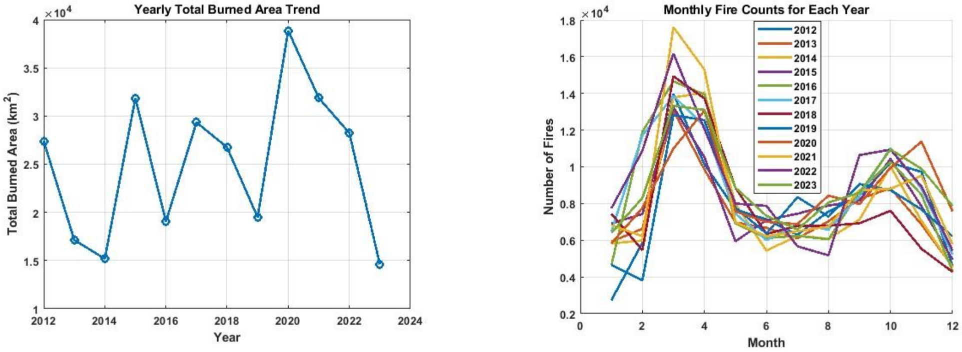

Figure 4 a) Time series for total area burned each year based on the CONFEX; b) Time series for number of fires each month across years in CONFEX

The regional trend of the number of fires in CONFEX reveals that the fire season is bimodal for the south with one peak in spring and the other in late fall (Figure 5 b). The west has a unimodal fire activity with peak lasting from late fall to early winter. Midwest has unimodal activity with spring peak, while the activity in northeast is uniform throughout the year with relatively more activity in summer but no clear peaks. The yearly area trend reveals that the west has the most burnt area followed by the south and midwest, respectively (Figure 5 c). The northeast has the lowest fire activity of the four regions.

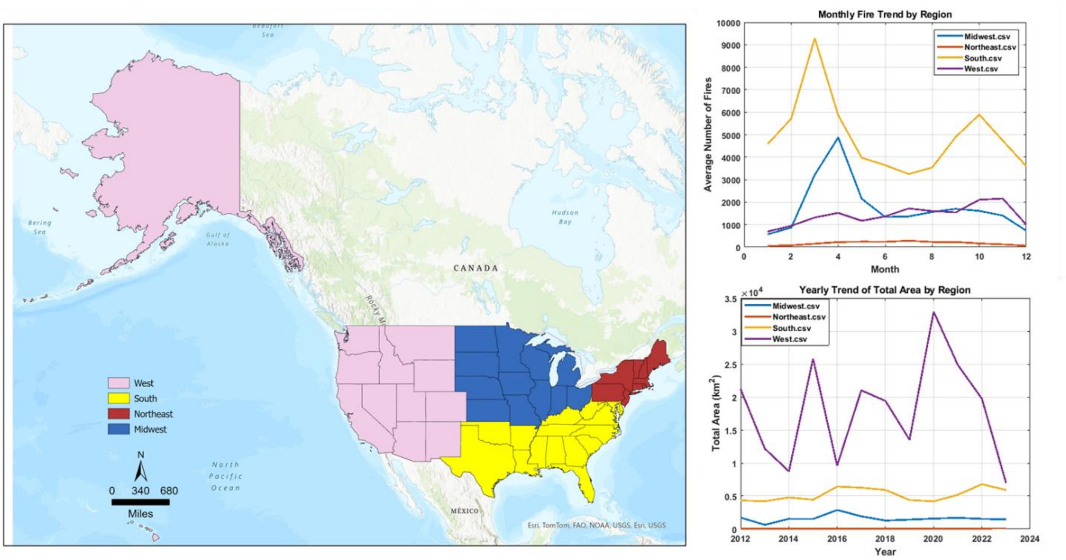

Figure 5 a) Different regions of CONUS and Alaska. b) Regional monthly trend of number of fires for CONUS and Alaska regions, based on CONFEX. c) Timeseries for total area burnt for different regions of CONUS and Alaska regions based on CONFEX.

In Figure 6, it is possible to see an example of fire perimeter and attributes for the Caldor fire. As per CALFIRE, the area burnt in Caldor was 897.73 Km^2 which is 6.7% lower than the 962.1 Km^2 observed through CONFEX (Caldor Fire | CAL FIRE). The CALFIRE provides a temporal span of the Caldor fire from 8/14/2021 to 10/21/2021 while CONFEX from 8/15/2021 to 10/05/2021. The alpha shape is supplemented by the various attributes which are available for every shape file or cluster. The number of points in each cluster is also presented, to provide an estimate of the number of hotspots detected by VIIRS in that cluster.

The CONFEX contains individual shape files of all the fires from 2012 to 2023, as captured by VIIRS S-NPP 375 m. The final product contains a csv file summary of all the fires, which can be readily used in ignition modelling.

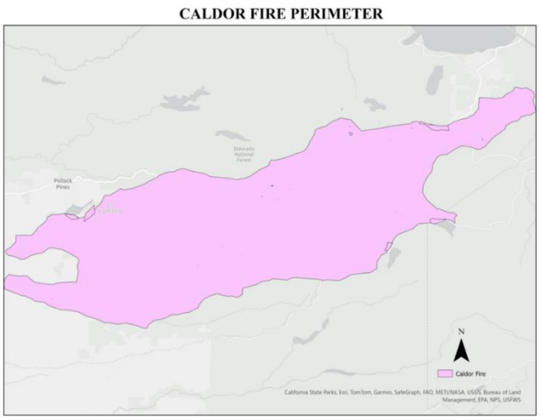

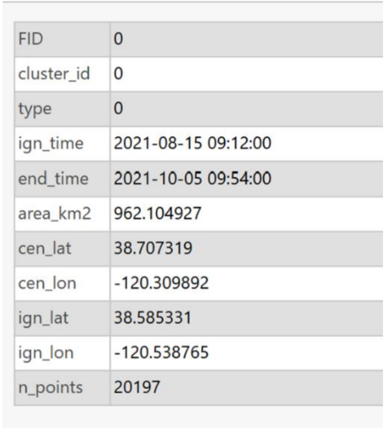

FID	0
cluster_id	0
type	0
ign_time	2021-08-15 09:12:00
end_time	2021-10-05 09:54:00
area_km2	962.104927
cen_lat	38.707319
cen_lon	-120.309892
ign_lat	38.585331
ign_lon	-120.538765
n_points	20197

Figure 6 Database example for Caldor fire California (Aug – Oct 2021).

We compared the fire perimeter of three large fires, Caldor, North Complex, and Soberanes, from CONFEX with the Department of Forestry and Fire Protection's Fire and Resource Assessment Program (FRAP) California database (data.ca.gov/dataset/California-fire-perimeters-1950) (Figure 7). We computed a confusion matrix by creating a bounding box around the two perimeters and we showed the results in Figure 8 and Table 1. The bounding box was divided into 0.01° by 0.01° cells and based on that a confusion matrix was developed. These are just three examples, and the database is enormous (1,202,150) and individual results may vary; however, these examples gave very satisfactory results.

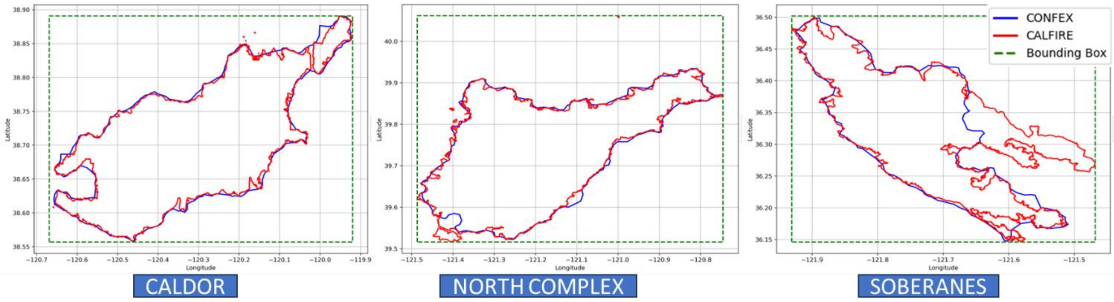

Figure 7 Comparison of perimeters from CONFEX and California Fire Department (CALFIRE) for Caldor, North complex, and Soberanes fires with respect to bounding boxes for confusion matrix analysis.

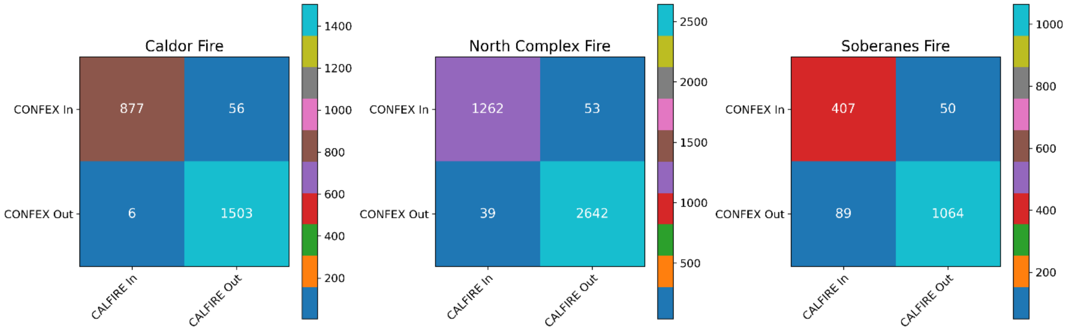

Figure 8 Confusion Matrices for the three fires depicted above.

Table 1 True Positive Rate, False Positive Rate, True Negative Rate, False Negative Rate, F1 score, Critical Success Index for the confusion matrices above, for the three fires.

Fire Name	**TPR**	**FNR**	**TNR**	**FPR**	**F1 Score**	**CSI**
Caldor	99.3%	0.7%	96.4%	3.6%	96.6%	93.4%
North Complex Fire	97.0%	3.0%	98.0%	2.0%	96.5%	93.2%
Soberanes	82.0%	18.0%	95.5%	4.5%	85.4%	74.5%

The TPR values range from 82 – 99% and indicate that the clustering process was able to correctly capture the majority of the three fires. The TNR values from 95 – 98% show that whenever there was no fire, there was no false detection, or the algorithm did not incorporate pixels of a different fire. The FNR value varies from 0.7 – 18%, the high value was in case of Soberanes fire, in which the algorithm was not able to detect a considerable portion of the fire, which is detected as a separate fire cluster, since the clustering process was based on the entire database. However, looking at the F1 score, CSI shows a good overall performance of the algorithm in classifying the pixels in right clusters.

4. Data Availability

The data set presented in this work is available on Mendeley data repository. The DOI for the dataset is 10.17632/sk6jwy7xmg.2 (Qadiri and Cerrai, 2025).

5. Conclusion

In this article we defined a new wildfire database for the CONUS and Alaska regions. The CONFEX database is based on the VIIRS S-NPP 375m satellite data product. Currently available datasets are either spatially inconsistent or lack perimeter information or are based on low resolution satellite products. The CONFEX database was created to address these gaps by using a high resolution VIIRS S-NPP 375m data product. The final product contains the perimeter, start date, end date, ignition and centroid location of the wildfires. The algorithm we developed takes the hotspot data and clusters it into actual fires over the specified region by using DBSCAN clustering, based on custom metrics. When compared with already available fire extents for three well known fires, we attained an F1 score of 85.5 – 96.6 % and a CSI of 73.5 – 93.4 %, showcasing the efficacy of the algorithm in classifying the hotspots. The CONFEX database has the potential to become an important asset for researchers looking for a comprehensive, high-resolution product for the CONUS and Alaska regions.

Acknowledgements

This research was funded by the Center for Weather Innovation and Smart Energy and Resilience (WISER) Industry Advisory Board. This research was also supported by the Eversource Energy Center.

References

Santín, Cristina, et al. "Pyrogenic organic matter production from wildfires: a missing sink in the global carbon cycle." Global Change Biology 21.4 (2015): 1621-1633.

Marks-Block, Tony, and William Tripp. "Facilitating prescribed fire in Northern California through Indigenous governance and interagency partnerships." Fire 4.3 (2021): 37.

Greenler, S. M., Lake, F. K., Tripp, W., McCovey, K., Tripp, A., Hillman, L. G., ... & Bailey, J. D. (2024). Blending Indigenous and western science: Quantifying cultural burning impacts in Karuk Aboriginal Territory. Ecological Applications, e2973.

Martinez, D. J., Seraphin, B., Marks-Block, T., Nelson, P., & Vinyeta, K. (2023). Indigenous fire futures: Anticolonial approaches to shifting fire relations in California. Environment and Society, 14(1), 142-161.

Copes-Gerbitz, K., Sutherland, I. J., Dickson-Hoyle, S., Baron, J. N., Gonzalez-Moctezuma, P., Crowley, M. A., ... & Burr, J. (2024). Guiding principles for transdisciplinary and transformative fire research. Fire Ecology, 20(1), 12.

Westerling, A. L. (2016). Increasing western US forest wildfire activity: sensitivity to changes in the timing of spring. Philosophical Transactions of the Royal Society B: Biological Sciences, 371(1696), 20150178.

Harvey, B. J. (2016). Human-caused climate change is now a key driver of forest fire activity in the western United States. Proceedings of the National Academy of Sciences, 113(42), 11649-11650.

Westerling, A. L., Hidalgo, H. G., Cayan, D. R., & Swetnam, T. W. (2006). Warming and earlier spring increase western US forest wildfire activity. science, 313(5789), 940-943.

Iglesias, V., Balch, J. K., & Travis, W. R. (2022). US fires became larger, more frequent, and more widespread in the 2000s. Science advances, 8(11), eabc0020.

Holden, Z. A., Swanson, A., Luce, C. H., Jolly, W. M., Maneta, M., Oyler, J. W., ... & Affleck, D. (2018). Decreasing fire season precipitation increased recent western US forest wildfire activity. Proceedings of the National Academy of Sciences, 115(36), E8349-E8357.

Brown, T. J., Hall, B. L., & Westerling, A. L. (2004). The impact of twenty-first century climate change on wildland fire danger in the western United States: an applications perspective. Climatic change, 62, 365-388.

Barbero, R., Abatzoglou, J. T., Steel, E. A., & Larkin, N. K. (2014). Modeling very large-fire occurrences over the continental United States from weather and climate forcing. *Environmental research letters*, *9*(12), 124009.

Wieting, C., Ebel, B. A., & Singha, K. (2017). Quantifying the effects of wildfire on changes in soil properties by surface burning of soils from the Boulder Creek Critical Zone Observatory. Journal of Hydrology: Regional Studies, 13, 43-57.

Taylor, S. W., Walsworth, N., & Anderson, K. (2024). Mapping Variable Wildfire Source Areas Through Inverse Modeling. Fire, 7(12), 454.

Barzani, A. R., Pahlavani, P., Ghorbanzadeh, O., Gholamnia, K., & Ghamisi, P. (2024). Evaluating the Impact of Recursive Feature Elimination on Machine Learning Models for Predicting Forest Fire-Prone Zones. Fire, 7(12), 440.

Syphard, A. D., Velazco, S. J. E., Rose, M. B., Franklin, J., & Regan, H. M. (2024). The importance of geography in forecasting future fire patterns under climate change. Proceedings of the National Academy of Sciences, 121(32), e2310076121.

Tong, H., Yuan, J., Zhang, J., Wang, H., & Li, T. (2024). Real-time wildfire monitoring using low-Altitude Remote sensing imagery. Remote Sensing, 16(15), 2827.

Zhao, Y., & Ban, Y. (2025). Near real-time wildfire progression mapping with VIIRS time-series and autoregressive SwinUNETR. International Journal of Applied Earth Observation and Geoinformation, 136, 104358.

Briley, A. A., & Afghah, F. (2024, May). Hardware acceleration for real-time wildfire detection onboard drone networks. In IEEE INFOCOM 2024-IEEE Conference on Computer Communications Workshops (INFOCOM WKSHPS) (pp. 01-06). IEEE.

Hu, H., Deng, X., Zhang, G., Feng, L., Long, J., Li, Z., ... & Wang, Y. (2024). Fire behavior simulation of Xintian forest fire in 2022 using WRF-fire model. Frontiers in Forests and Global Change, 7, 1336716.

Sadrabadi, M. T., & Innocente, M. S. (2024). Enhancing wildfire propagation model predictions using aerial swarm-based real-time wind measurements: A conceptual framework. Applied Mathematical Modelling, 130, 615-634.

Pereira, J., Mendes, J., Júnior, J. S., Viegas, C., & Paulo, J. R. (2024). Metaheuristic algorithms for calibration of two-dimensional wildfire spread prediction model. Engineering Applications of Artificial Intelligence, 136, 108928.

Porter, T. W., Crowfoot, W., & Newsom, G. (2019). Wildfire Activity Statistics. California Department of Forestry and Fire Protection: Sacramento, CA, USA, 46.

Brown, T. J., Hall, B. L., Mohrle, C. R., & Reinbold, H. J. (2002). Coarse assessment of federal wildland fire occurrence data. Report for the National Wildfire Coordinating Group, CEFA Report, 02-04.

Short, K. C. (2022). Spatial wildfire occurrence data for the United States, 1992-2020 [FPA_FOD_20221014].

Barmpoutis, P., Papaioannou, P., Dimitropoulos, K., & Grammalidis, N. (2020). A review on early forest fire detection systems using optical remote sensing. Sensors, 20(22), 6442.

Dennison, P. E., & Roberts, D. A. (2009). Daytime fire detection using airborne hyperspectral data. Remote Sensing of Environment, 113(8), 1646-1657.

Hirsch, E., & Koren, I. (2021). Record-breaking aerosol levels explained by smoke injection into the stratosphere. *Science*, *371*(6535), 1269-1274.

Ma, C., Su, H., Lelieveld, J., Randel, W., Yu, P., Andreae, M. O., & Cheng, Y. (2024). Smoke-charged vortex doubles hemispheric aerosol in the middle stratosphere and buffers ozone depletion. *Science Advances*, *10*(28), eadn3657.

Encyclopedia Astronautix. (n.d.). *Tiros N.* [Archived version]. https://web.archive.org/web/20140624105104/http://www.astronautix.com/craft/tirosn.htm

Warren, J. R., & Wilson, R. A. (1981). Airborne Infrared Forest Fire Surveillance: A Chronology of USDA Forest Service Research and Development (Vol. 115). US Department of Agriculture, Forest Service, Intermountain Forest and Range Experiment Station.

Warneke, C., Schwarz, J. P., Dibb, J., Kalashnikova, O., Frost, G., Al-Saad, J., ... & FIREX-AQ Science Team. (2023). Fire influence on regional to global Environments and air quality (FIREX-AQ). Journal of Geophysical Research: Atmospheres, 128(2), e2022JD037758.

Veraverbeke, S., Dennison, P., Gitas, I., Hulley, G., Kalashnikova, O., Katagis, T., ... & Stavros, N. (2018). Hyperspectral remote sensing of fire: State-of-the-art and future perspectives. *Remote Sensing of Environment*, *216*, 105-121.

https://doi.org/10.5194/essd-2025-462
Preprint. Discussion started: 26 August 2025

Green, R. O., Eastwood, M. L., Sarture, C. M., Chrien, T. G., Aronsson, M., Chippendale, B. J., ... & Williams, O. (1998). Imaging spectroscopy and the airborne visible/infrared imaging spectrometer (AVIRIS). *Remote sensing of environment*, *65*(3), 227-248.

Itten, K. I., Dell'Endice, F., Hueni, A., Kneubühler, M., Schläpfer, D., Odermatt, D., ... & Meuleman, K. (2008). APEX-the hyperspectral ESA airborne prism experiment. *Sensors*, *8*(10), 6235-6259.

Nordin, M. S., & Aziz, F. A. (2007). Ground Receiving Station (GRS) of UMS–Receiving and Processing the Electromagnetic Wave Data from Satellite. J. Nucl. Relat. Technol., 4, 199-208.

DeBano, L. F. (1991, August). The effect of fire on soil properties. In Proceedings management and productivity of western-Montane. Forest Soils (pp. 151-155).

Bright, B. C., Hudak, A. T., Kennedy, R. E., Braaten, J. D., & Henareh Khalyani, A. (2019). Examining post-fire vegetation recovery with Landsat time series analysis in three western North American forest types. Fire Ecology, 15(1), 1-14.

Barbero, R., Abatzoglou, J. T., Steel, E. A., & Larkin, N. K. (2014). Modeling very large-fire occurrences over the continental United States from weather and climate forcing. *Environmental research letters*, *9*(12), 124009.

Giglio, L., & Kendall, J. D. (2001). Application of the Dozier retrieval to wildfire characterization: A sensitivity analysis. Remote sensing of Environment, 77(1), 34-49.

Leblon, B., San-Miguel-Ayanz, J., Bourgeau-Chavez, L., & Kong, M. (2016). Remote sensing of wildfires. In *Land surface remote sensing* (pp. 55-95). Elsevier.

Heyns, A., Du Plessis, W., Kosch, M., & Hough, G. (2019). Optimisation of tower site locations for camera-based wildfire detection systems. International journal of wildland fire, 28(9), 651-665.

Bao, S., Xiao, N., Lai, Z., Zhang, H., & Kim, C. (2015). Optimizing watchtower locations for forest fire monitoring using location models. Fire safety journal, 71, 100-109.

Allison, R. S., Johnston, J. M., Craig, G., & Jennings, S. (2016). Airborne optical and thermal remote sensing for wildfire detection and monitoring. Sensors, 16(8), 1310.

Prins, E. M., & Menzel, W. P. (1992). Geostationary satellite detection of bio mass burning in South America. *International Journal of Remote Sensing*, *13*(15), 2783-2799.

Space Science & Engineering Center (SSEC). (n.d.). *VAS (1980)*. University of Wisconsin–Madison. https://library.ssec.wisc.edu/digital-collections/research-history/vas-1980/

Kornei, K. (2020), Wildfires trigger long-term permafrost thawing, *Eos, 101*, https://doi.org/10.1029/2020EO148336. Published on 31 August 2020.

Kim, I. W., Timmermann, A., Kim, J. E., Rodgers, K. B., Lee, S. S., Lee, H., & Wieder, W. R. (2024). Abrupt increase in Arctic-Subarctic wildfires caused by future permafrost thaw. *Nature Communications*, *15*(1), 7868.

Li, X. Y., Jin, H. J., Wang, H. W., Marchenko, S. S., Shan, W., Luo, D. L., ... & Jia, N. (2021). Influences of forest fires on the permafrost environment: A review. *Advances in Climate Change Research*, *12*(1), 48-65.

Prins, E. M., & Menzel, W. P. (1994). Trends in South American biomass burning detected with the GOES visible infrared spin scan radiometer atmospheric sounder from 1983 to 1991. *Journal of Geophysical Research: Atmospheres*, *99*(D8), 16719-16735.

Kaufman, Y. J., Justice, C. O., Flynn, L. P., Kendall, J. D., Prins, E. M., Giglio, L., ... & Setzer, A. W. (1998). Potential global fire monitoring from EOS-MODIS. *Journal of Geophysical Research: Atmospheres*, *103*(D24), 32215-32238.

Cahoon Jr, D. R., Stocks, B. J., Levine, J. S., Cofer III, W. R., & O'Neill, K. P. (1992). Seasonal distribution of African savanna fires. *Nature*, *359*(6398), 812-815.

Xiong, X., King, M. D., Salomonson, V. V., Barnes, W. L., Wenny, B. N., Angal, A., ... & Link, D. O. (2015). Moderate resolution imaging spectroradiometer on Terra and Aqua missions. *Optical Payloads for Space Missions*, 53-89.

Giglio, L., Descloitres, J., Justice, C. O., & Kaufman, Y. J. (2003). An enhanced contextual fire detection algorithm for MODIS. Remote sensing of environment, 87(2-3), 273-282.

Giglio, L., Schroeder, W., & Justice, C. O. (2016). The collection 6 MODIS active fire detection algorithm and fire products. *Remote sensing of environment*, *178*, 31-41.

Giglio, Louis, et al. "MODIS collection 6 and collection 6.1 active fire product user's guide." National Aeronautical and Space Administration—NASA: Washington, DC, USA 64 (2021).

Xiong, X., & Butler, J. J. (2020). MODIS and VIIRS calibration history and future outlook. Remote Sensing, 12(16), 2523.

Justice, C. O., Román, M. O., Csiszar, I., Vermote, E. F., Wolfe, R. E., Hook, S. J., ... & Masuoka, E. J. (2013). Land and cryosphere products from Suomi NPP VIIRS: Overview and status. Journal of Geophysical Research: Atmospheres, 118(17), 9753-9765.

Xiong, X., Angal, A., Sun, J., Lei, N., Twedt, K., Chen, H., & Chiang, K. (2023). An overview of NOAA-21 VIIRS early on-orbit calibration and performance. Sensors, Systems, and Next-Generation Satellites XXVII, 12729, 308-317.

Cao, C., Blonski, S., Wang, W., Uprety, S., Shao, X., Choi, J., ... & Kalluri, S. (2018, November). NOAA-20 VIIRS on-orbit performance, data quality, and operational Cal/Val support. In Earth observing missions and sensors: Development, implementation, and characterization V (Vol. 10781, pp. 63-71). SPIE.

Schroeder, W., Oliva, P., Giglio, L., & Csiszar, I. A. (2014). The New VIIRS 375 m active fire detection data product: Algorithm description and initial assessment. Remote Sensing of Environment, 143, 85-96.

Schroeder, W., & Giglio, L. (2016). Visible Infrared Imaging Radiometer Suite (VIIRS) 375 m active fire detection and characterization algorithm theoretical basis document. University of Maryland: Washington, DC, USA.

Qadiri, Raja Zubair Zahoor; Cerrai, Diego (2025), "CONFEX: CONUS and Alaska Fire EXtent database", Mendeley Data, V2, doi: 10.17632/sk6jwy7xmg.2

Short, K. C., Finney, M. A., Scott, J. H., Gilbertson-Day, J. W., & Grenfell, I. C. (2016). Spatial dataset of probabilistic wildfire risk components for the conterminous United States. USDA Forest Service Research Data Archive. (Fort Collins, CO, USA) 10.2737. RDS-2016-0034.

National Aeronautics and Space Administration (NASA). (n.d.). *Fire Information for Resource Management System (FIRMS)*.

Artés, T., Oom, D., De Rigo, D., Durrant, T. H., Maianti, P., Libertà, G., & San-Miguel-Ayanz, J. (2019). A global wildfire dataset for the analysis of fire regimes and fire behaviour. Scientific data, 6(1), 296.

Chen, Y., Hantson, S., Andela, N., Coffield, S. R., Graff, C. A., Morton, D. C., ... & Randerson, J. T. (2022). California wildfire spread derived using VIIRS satellite observations and an object-based tracking system. Scientific data, 9(1), 249.

Kaufman, Y. J., Justice, C. O., Flynn, L. P., Kendall, J. D., Prins, E. M., Giglio, L., ... & Setzer, A. W. (1998). Potential global fire monitoring from EOS-MODIS. Journal of Geophysical Research: Atmospheres, 103(D24), 32215-32238.

Giglio, L., Descloitres, J., Justice, C. O., & Kaufman, Y. J. (2003). An enhanced contextual fire detection algorithm for MODIS. Remote sensing of environment, 87(2-3), 273-282.

Boschetti, L., Roy, D., Hoffmann, A. A., & Humber, M. (2009). MODIS Collection 5 Burned Area Product-MCD45. User's Guide, Ver, 2, 1-2.

Elvidge, C. D., Zhizhin, M., Hsu, F. C., & Baugh, K. E. (2013). VIIRS nightfire: Satellite pyrometry at night. Remote Sensing, 5(9), 4423-4449.